 doi:10.20944/preprints201810.0631.v1

Article

Detection of nonspecific binding of *E. coli* O157:H7 on reduced graphene oxide screen-printed carbon electrodes using electrochemical methods

Nur Alya Batrisya Ismail, Nasteho Ali Ahmed, Firdaus Abd-Wahab, Nurul Izzati Ramli, Wan Wardatul Amani Wan Salim*

Department of Biochemical and Biotechnology Engineering, Kulliyyah of Engineering
International Islamic University Malaysia, 50728 Gombak, Kuala Lumpur, Malaysia.

* Correspondence: asalim@iium.edu.my; Tel.: +6016-4445364

Abstract:

Immunosensors have been widely developed to use antibodies to detect a pathogen of interest; it is interesting to look at the effect of nonspecific antibody binding to *E. coli* using electrochemical methods. IgG antibody not specific to *E. coli* O157:H7 was crosslinked onto a screen-printed carbon electrode. The presence of *E. coli* at 4, 4×10^2, 4×10^5, and 4×10^8 CFU/ml on the electrode surface was detected via linear sweep voltammetry (LSV) and electrochemical impedance spectroscopy (EIS). Current transfer at both electrodes was reduced as the concentration of bacteria increased; however, the calibration of number of cells to decreased current was nonlinear for IgG-modified electrodes. The nonlinearity is confirmed by EIS measurements which showed highest impedance at 4 CFU/ml *E. coli* when impedance should be the lowest. FESEM images showed higher binding of cells when IgG is present compared to electrodes with reduced graphene oxide (rGO) alone. Electrodes with rGO alone show less attachment of *E. coli*, with EIS showing a linear calibration profile, while LSV shows not much difference in current values for all concentrations aside from the highest concentration. These results suggest that nonspecific binding can provide false signals in electrochemical measurements, and it is crucial to provide proper controls.

Keywords: *E. coli* O157:H7; IgG; nonspecific binding; reduced graphene oxide; linear sweep voltammetry; electrical impedance spectroscopy

1. Introduction

Detection methods for pathogenic microorganisms with no requirement for trained laboratory personnel or laboratory space is important for water surveillance purpose during post-flood efforts so informed decisions can be made to improve sanitation standards and water infrastructure. Electrochemical biosensors best fit the requirement for diagnostic devices as outlined by WHO: they are to be made ASSURED – affordable, sensitive, specific, user-friendly, rapid and robust, equipment-free and deliverable [1] to end users for pathogen detection. Developments in material science and surface chemistry aim to improve electrochemical biosensors in their specificity, sensitivity, and detection limit by introducing new biorecognition schemes and enhanced electrode conductivity with electrocatalytic ability.

 doi:10.20944/preprints201810.0631.v1

Owing to the need to distinguish pathogenic microorganisms from non-pathogenic ones, electrochemical biosensors can employ various biorecognition schemes such as DNA/RNA/PNA [2–4], antibody [5–7], aptamers [8–10], antimicrobial peptides [11–13], carbohydrate [14,15] and bacteriophages [16–18]. In bacteria detection, specificity to identify pathogenic bacteria strains that can cause illness is vital. The antigen-antibody pair can provide such specificity to detect a virulent pathogenic *Escherichia coli* strain owing to the ability of antibody to detect very low cell numbers and provide the sensitivity needed for a biosensor. *E. coli* has over 700 serotypes; *E. coli* O157:H7 is one of the pathogenic serotypes that produce Shiga toxins and is one of the microorganisms most adaptable to changing environment. Shiga toxin is responsible for bloody diarrhea and hemolytic uremic syndrome (HUS); the latter is characterized by kidney and renal failure and anemia [19,20]. *E. coli* O157:H7 is often the cause of serious outbreaks of foodborne illness. Infections are often transmitted by animals to food crops through irrigation and contaminated water, manure [21], and air and biological dispersions of biological vectors [22]. These outbreaks become more serious when flooding occurs in rural areas – as is the case in East Coast Malaysia [23], where water supply and sanitation system are disrupted, causing serious waterborne diseases. Since virulent pathogens such as *E. coli* O157:H7 often occur in low numbers in food or water samples, detection methods need to be not only specific but also need to be sensitive, with a low limit of detection. ASSURED devices are important during post-flood efforts to detect pathogenic *E. coli* so that contaminated water can be effectively treated.

To address the sensitivity and detection limit of ASSURED biosensors, antibodies for biosensor biorecognition sites require a very specific epitope to the *E. coli* strain, because many strains share the same surface proteins with similar homologs that can lead to nonspecific binding. Furthermore, the antibody should have high affinity to the antigen of interest [5]. A necessary characteristic of an ASSURED biosensor for specific pathogenic microorganism detection is the blocking of other microorganisms on the biosensor surface; electrochemical detection methods are not able to distinguish between dead and viable cells, or between the specific strains of interest. Many studies using electrochemical methods for biorecognition of a specific antigen-antibody scheme have shown ability to detect one cell of *E. coli* O157:H7, over a wide linear range [24]. Of interest to us is using electrochemical methods to study antigen-antibody binding when the antibody used is not specific to *E. coli* O157:H7. In our work, IgG (immunoglobulin G or γ) not specific for *E. coli* O157:H7 was used to study how nonspecific binding can affect measurements made by electrochemical biosensors fabricated from screen printed carbon electrodes (SPCEs).

IgG is a four-chain glycoprotein monomer linked at the inter-heavy chains by a disulfide bond to form the typical Y-shaped antibody conformation [25,26]. It consists of two identical heavy chains and two identical light chains. IgG is one of the five classes of immunoglobulin that can be found in mammals, including humans. It is expressed up to 75% of the serum content in human, making it the major constituent of all human immunoglobulins [27]. This abundance can be attributed to its key role as an opsonin, or the antibody that protects its host against foreign microorganisms. Upon detecting the presence of a foreign body, such as a bacterium, the expressed IgGs will typically bind to the outer surface of the bacterium and coat the cellular surface, before activating the phagocytic pathway that will eventually ingest the microorganism [26].

IgG has been shown to bind bacterial cells through its recognition of the outer membrane constituents of the bacteria, such as membrane proteins and lipopolysaccharides [25,28]. Recognition and binding specificity of the antibody to these constituents rely on the adaptability of the variable domains at the antigen-binding site of the antibody to the antigens present at the outer membrane layer of the bacteria. The lack of specific expression of IgG against a particular bacterium would thus result in recognition with lower specificity towards a common recognizable constituent present on the cellular surface of a bacteria, particularly of the O-antigen of the bacterial lipopolysaccharide.

Preprints (www.preprints.org) | NOT PEER-REVIEWED | Posted: 26 October 2018 doi:10.20944/preprints201810.0631.v1

Electrochemical detection methods used to detect bacteria are cyclic voltammetry (CV), linear sweep voltammetry (LSV), differential pulse voltammetry (DPV), amperometry, and electrical impedance spectroscopy (EIS). The detection methods are based on measurements of current or voltages from ions that are transduced at the biorecognition sites at the electrode-solution interface [24]. For ASSURED devices, a three-electrode system of screen-printed carbon electrode (SPCE) fitted to a portable platform like a smartphone best addresses the requirements [29]. In our work, we used a commercially available SPCE and modified the working electrodes (WEs) with reduced graphene oxide (rGO) with increased surface area for antibody immobilization [30]. The high surface area of the rGO can be further enhanced with gold nanoparticles (AuNPs) to increase sensitivity, whose improvement can be seen from the increased peak current in cyclic voltammetry (CV) graphs. We studied the effect of rGO-based composites on the CV peak current and found that rGO could be easily modified with other materials to tune its electrochemical properties [31]. In this work, we utilized rGO with exposed carboxyl groups without further surface modification for antibody immobilization; IgG was used to bind to the exposed carboxyl group of rGO.

The mechanism of *E. coli* O157:H7 detection is shown in Figure 1; IgG not specific for *E. coli* O157:H7 was immobilized on rGO-modified SPCE WEs and exposed to *E. coli* O157:H7. The detection principle is based on the amount of current successfully transduced from the bulk solution to the electrode surface, where the presence of *E. coli* cells is known to inhibit the current flow. Based on this principle, we employed two methods of detection: linear sweep voltammetry (LSV) in potable tap water and electrical impedance spectroscopy (EIS) in phosphate buffer saline (PBS) containing potassium ferricyanide/ferrocyanide as redox probe.

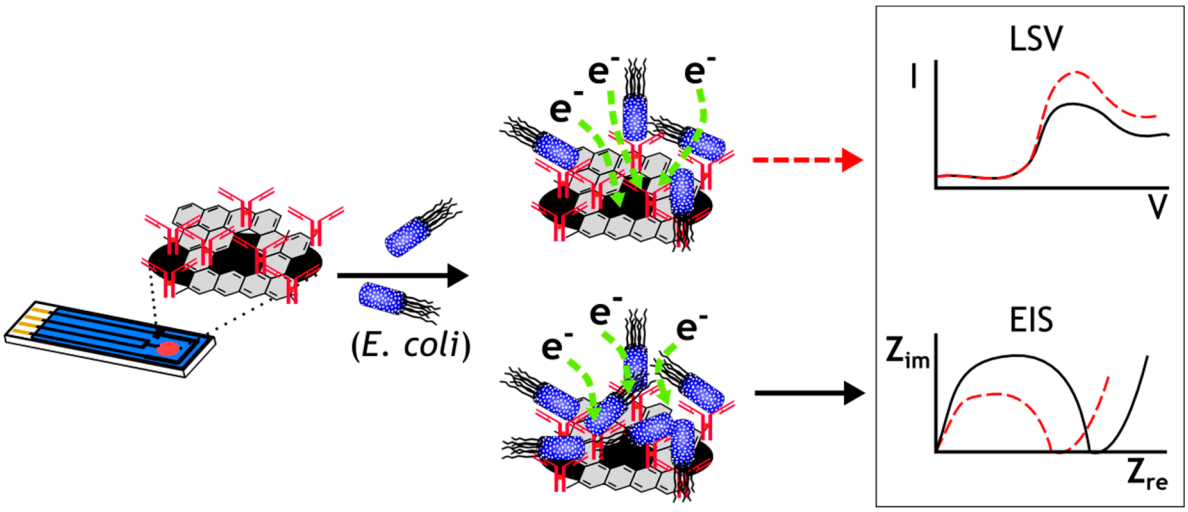

Figure 1 Immunosensor detection mechanism. The IgG rabbit serum immobilized on the electrode is exposed to the target analyte (*E. coli* O157:H7) to form an antibody-antigen complex on the electrode surface. Electrochemical detection was done using linear sweep voltammetry (LSV) and electrochemical impedance spectroscopy (EIS). Electrons that are successfully transduced through the electrode surface are reported as current (I) plotted against voltage (V). For measurable detection, the electrons must penetrate the layer formed by the antibody-antigen complex. The EIS measures the resistive behavior against electrochemical reaction at the interface layer proportional to the presence of cells. The real (Z_{re}) and imaginary (Z_{im}) parts of the impedance are plotted. The more *E. coli* O157:H7 that is bound specifically to the antibody, the fewer the ions that could rapidly diffuse between the bulk solution and the electrode and be transduced across the electrode surface. This is reflected by the lower magnitude of peak current seen in the LSV, and the higher impedance seen in the EIS. The red dashed line represents the LSV and EIS profiles from electrodes with fewer cells attached to the electrode surface, whereas the black solid lines represent higher number of cells attached.

 doi:10.20944/preprints201810.0631.v1

The LSV method measures current with a forward voltage sweep, thus causing ions from potable tap water to be transduced across the electrode surface into measurable electrons and data are plotted as current (I) against voltage (V). The magnitude of current measured is proportional to the electrons being transduced; any insulative barrier causes fewer electrons to be transduced [33,34]. In our work, *E. coli* O157:H7 cells that successfully attached to the electrode surface acted as such a barrier, blocking exposed electrode surface to the bulk solution [35]. EIS measures impedance at the electrode-bulk solution interface where the real (Z′) and imaginary (Z″) components of impedance are plotted; more *E. coli* cells attached to the electrode surface result in higher impedance. The impedance at the electrode–bulk solution interface can be represented by a Randles equivalent circuit model, from which a Nyquist plot can be obtained. From the Nyquist plot, impedance at the electrode–bulk solution interface, charge-transfer resistance, and Warburg impedance can be determined [36,37].

We aim to understand the effect of *E. coli* O157:H7 cell attachment on immobilized IgG not specific for *E. coli* O157:H7 by looking at the current transfer and the corresponding impedance at the electrode–-bulk solution interface, with verification of cell attachment on electrodes from field-emission scanning electron microscope (FESEM) imaging. *E. coli* O157:H7 cells with concentration ranges from 4 to 4 × 10^8 CFU/ml were used to see the effect of cell concentration on cell attachment. Understanding the effect of *E. coli* O157:H7 cell attachment on electrode surface modified with IgG not specific to the strain can help us better understand the effect of nonspecific binding on current transfer and impedance, thus allowing us to analyze the advantages and limitations of LSV and EIS in the detection and quantification of *E. coli*, provide better strategies for antibody immobilization on electrode surfaces, and inform the design of microfluidics devices for controlled delivery of cells on electrode surfaces. In real situations, use of food or water contaminated with bacteria requires an appropriate pretreatment process before the sensing step. Pretreatment by dispersion, filtration, suitable pH, and bacteria flow across the electrode surface should be designed in accordance with water quality–monitoring guidelines.

2. Materials and Methods

2.1 Materials and reagents

Ultra-highly concentrated single-layer graphene oxide (UHC-GO-60) solution was purchased from Graphene Supermarket (Richmond, NY, USA). Potassium ferricyanide ($K_3Fe(CN)_6$), potassium ferrocyanide ($K_4Fe(CN)_6{\cdot}3H_2O$), phosphate buffered saline (PBS, pH 7.4) tablets, sulfuric acid (H_2SO_4), hydrochloric acid (HCl), N-hydroxysulfosuccinimide (NHS), 1-ethyl-3-(3-dimethylaminopropyl) carbodiimide (EDC), IgG from rabbit serum (I5006) were all purchased from Sigma-Aldrich, St. Louis, MO 63103, USA. PBS tablets were dissolved in deionized water and the pH was adjusted by addition of hydrochloric acid (HCl). Heat-killed *Escherichia coli* serotype O157:H7 cells in dextran solution (50-95-90) with cell count of 3.98 × 10^9 CFU/ml was purchased from Kirkegaard and Perry Lab (KPL) Inc., Gaithersburg, MD, USA. Tap water was collected directly from the taps in our laboratory. Screen-printed carbon electrodes (SPCEs) with working electrodes (WEs) 2 mm in diameter (Ø = 2 mm) were purchased from Pine Instrument, Grove City, PA. The reference electrode (RE) is Ag/AgCl and the counter electrode (CE) is similar to the WE. Deionized water was used throughout this study unless stated otherwise.

2.2 Instrumentation

Electrochemical measurements were performed using a three-electrode pocketSTAT (IVIUM Technologies, Eindhoven, the Netherlands) at ambient temperature. The results were analyzed using IviumSoft software. Morphological change in the modified electrodes at each fabrication step and different *E.coli* concentration was observed via field emission scanning electron microscopy (FESEM)

 doi:10.20944/preprints201810.0631.v1

using a Hitachi SU8020 UHR Cold-Emission FESEM available at MIMOS Technology Solutions, Sdn. Bhd., Seri Kembangan, Selangor, Malaysia.

2.3 *Fabrication of immunosensors (IgG/rGO/GCE) and E. coli detection*

Figure 2 summarizes the fabrication steps of the immunosensors for the detection of *E. coli* O157:H7. The SPCEs were pretreated and activated via cyclic voltammetry (CV) for 3 cycles in 0.1 M H_2SO_4 solution with an anodic potential of 2.5 V to -2.5 V and a scan rate of 100 mV/s [38,39]. Following activation, the electrodes were rinsed with DI water and dried at ambient temperature. Three µl GO (6.2 g/l) was dropcast onto a pretreated SPCE and dried at ambient temperature for 2 hours (denoted as GO/SPCE). Then the GO/SPCE was reduced electrochemically to rGO/SPCE via CV in PBS, pH 5.0, using a potential range from 0 V to -1.5 V and scan rate of 100 mV/s for 5 cycles to remove -OH functional groups while retaining –COOH functional groups for antibody binding [40,41].

Immunoglobulin G (IgG) antibodies from rabbit serum were immobilized on the rGO/SPCE via covalent bonding of the carboxyl groups on the rGO surface and the amine groups of IgG to produce IgG/rGO/SPCE. All electrodes were exposed to 3 µl of a 1:1 mixture of 1-ethyl-3-(3-dimethylaminopropyl) carbodiimide (EDC; 0.5 M) and N-hydroxysulfosuccinimide (NHS; 0.1 M) and incubated at 37 °C for 20 min to activate carboxyl functional groups (-COOH) on the rGO surface. Three (3) µl of IgG from rabbit serum (2 µg/ml) was added to the rGO/SPCE and incubated at 37 °C for 2 hours. The unbound IgG was washed off by rinsing the electrodes with PBS, pH 7.1. Finally, the IgG/rGO/SPCEs were exposed to the *E. coli* O157:H7 cells in tap water at various concentration and characterized electrochemically via LSV and EIS.

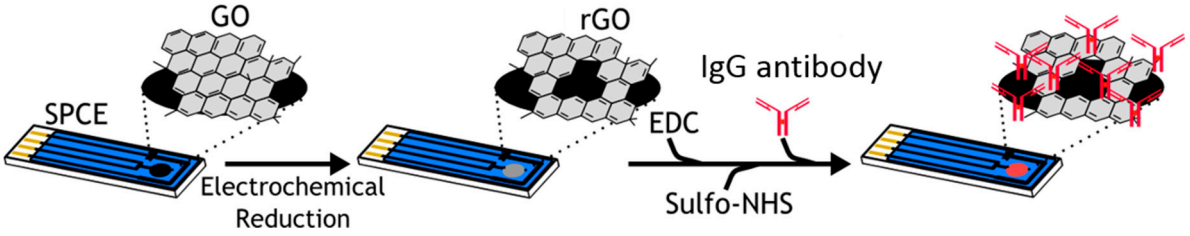

Figure 2 Fabrication steps of the immunosensor for the detection of *E. coli* O157:H7. A precleaned bare screen-printed carbon electrode (SPCE) was used as a conductive substrate onto which 3 µl graphene oxide (GO) was drop-cast, producing a layer of GO on the SPCE (GO/SPCE). The electrical conductivity of GO was restored by electrochemical reduction, which removes most oxygenated functional groups and leaves mostly carboxyl groups. This results in the formation of reduced graphene oxide (rGO) on the SPCE. Subsequent immobilization of IgG not specific for the *E. coli* strain on the rGO-modified electrode was done through a carbodiimide-assisted amidation reaction mediated by sulfo-NHS and EDC.

2.4 *Linear Sweep Voltammetry (LSV) measurements*

For detection of *E. coli*, 3 µl PBS, pH 7.1, containing a certain concentratio of *E. coli* O157:H7 was drop-cast onto the IgG/rGO/GCE and incubated at 37 °C for 1 hour. After multiple gentle washings with PBS, pH 7.1, LSV measurements were performed in tap water at a potential range of -0.5 V to 1 V with scan rate of 100 mV/s. Electrodes were treated with different *E. coli* concentrations (4×10^8, 4×10^5, 4×10^2, and 4×10^0 CFU/ml) and LSV was performed to see changes in I_{pa} and to observe the limit of detection (LOD).

 doi:10.20944/preprints201810.0631.v1

2.5 Electrical Impedance Spectroscopy (EIS) measurements

EIS was performed in 0.01 M PBS, pH 7.1, containing 5 mM $K_3Fe(CN)_6$:$K_4Fe(CN)_6$ (1:1) as redox probe, with current range of 10 μA, amplitude of 20 mV, and frequency range of 100 kHz to 0.1 Hz [12]. The measured EIS spectrum was fitted with Randles equivalent circuit in an Ivium Equivalent Circuit Evaluator. The equivalent circuit compares and analyzes the experimental impedance with the typical ideal impedance. In our case, the Randles equivalent circuit is used as our model to analyze the solution resistance, charge-transfer resistance, double-layer capacitance, and Warburg impedance. The frequency dependence of the impedance reveals the underlying chemical process at the electrode surface.

2.6 Binding of E. coli O157:H7 to reduced graphene oxide electrode modified with IgG

FESEM at 5K magnification was used to verify the binding of *E. coli* to the electrode surface. Imaging was conducted at all four quadrants of an SPCE working-electrode surface to ensure that all the surface were imaged.

3. Results and Discussions

3.1 Linear sweep voltammetry of screen-printed carbon electrodes at different fabrication steps

The LSVs of bare SPCE, GO/SPCE, rGO/SPCE, and IgG/rGO/SPCE have been conducted in tap water to understand the current transfer at each fabrication step. The LSVs were run from -0.5 V to 1 V with scan rate 100 mV/s, and the results were plotted as a I-V voltammogram, as shown in Figure 3. Current above the potential -0.2 V shows GO/SPCE with the lowest current, close to zero, while rGO/SPCE shows the highest current. Furthermore, the immobilization of IgG on the rGO surface (IgG/rGO/SPCE) lowers the current to a level close to that of GO/SPCE.

The low current of GO/SPCE is a result of damaged sp^2 carbon lattices and abundance of oxygenated GO groups contributing to its poor electrical conductivity [42–44]. However, when GO was reduced to rGO, the sp^2 lattice was partially restored and some attached oxygenated groups were removed, resulting in rGO/SPCE's having the highest current. The lower current of IgG/rGO/SPCE in comparison with rGO/SPCE implies that IgGs are immobilized on the electrode. It is important to note here that studies have shown that protein in dry and wet states is semiconductive [45], so current can still be transferred across the IgG to the conductive electrode surface. In addition, the conductivity of antibody is based on its structure, and the way in which it is immobilized on the electrode surface [46].

After the 0.2 V potential point, all graphs exhibit a linear profile, whose slopes are 0.035, 0.025, 0.033 and 0.029 for SPCE, GO/SPCE, rGO/SPCE and IgG/rGO/SPCE, respectively. This shows that tap water as the electrolyte is stable up to 1 V without electrochemical reaction occurring, enabling the electrode to be used as an immunosensor when measurements are made in weak electrolyte solutions such as tap water [47].

Preprints (www.preprints.org) | NOT PEER-REVIEWED | Posted: 26 October 2018 doi:10.20944/preprints201810.0631.v1

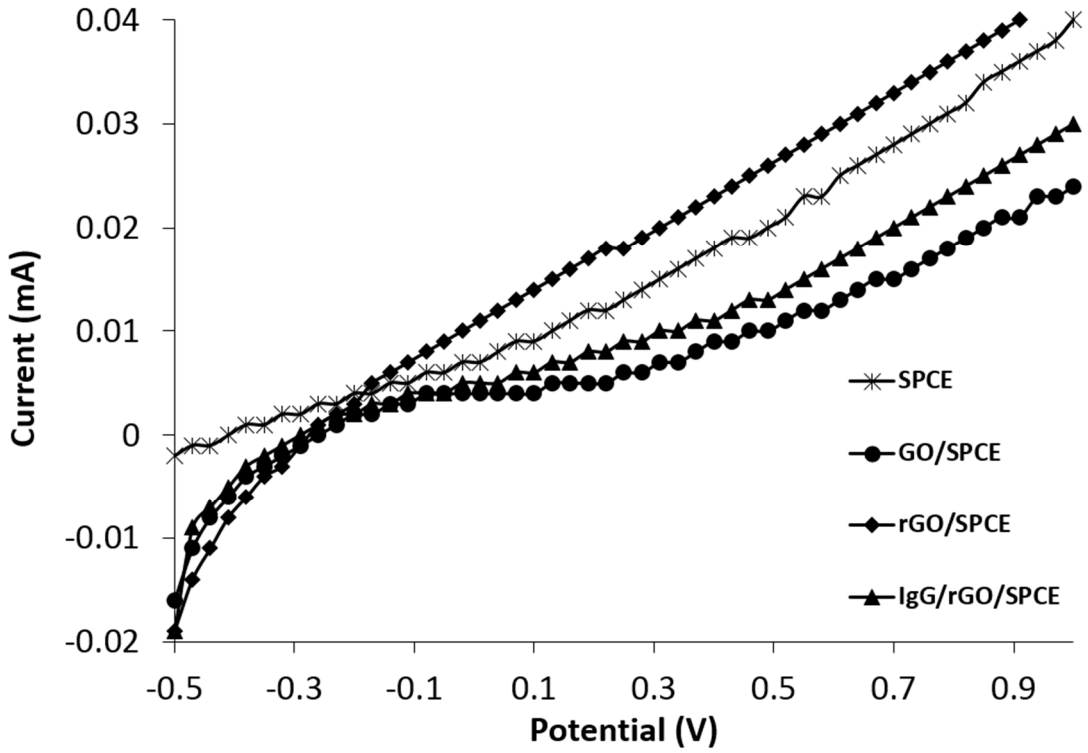

Figure 3 Linear sweep voltammetry (LSV) results at different fabrication steps (bare SPCE, GO/SPCE, rGO/SPCE and IgG/rGO/SPCE) at a scan rate of 100 mV/s in tap water. The figure indicates the electron-transfer behavior on the electrode surface as the sweep was run at a potential of -0.5 V to 1 V. GO/SPCE exhibits the lowest current and rGO exhibits the highest current after -0.2 V. The slopes of the graphs in the linear region are 0.035, 0.025, 0.033 and 0.029 for SPCE, GO/SPCE, rGO/SPCE and IgG/rGO/SPCE, respectively.

3.2 EIS of screen-printed carbon electrode at different fabrication steps

EIS is typically used to analyze interfacial behavior occurring at modified electrode surfaces. The impedance measurement for an immunosensor is highly dependent on the species adsorbed on the electrode surface. In a standard Nyquist plot, two obvious regions are observed at low and high frequency; in the high frequency region, a semicircular plot is observed, which indicates a charge transfer–limited process (faradaic phenomenon). In the low frequency region, a linear curve is observed, which indicates the mass transport of a diffusion-limited process (non-faradaic phenomenon), thus removing the contribution of convection and migration. As planar electrodes are used throughout this study, the concentration of redox and oxidized species can be represented by Fick's law of diffusion, where species diffuse perpendicularly to the planar electrodes in the x direction. Since the electrodes used are based on Fick's law, prediction of species concentration as a function of time can be made [48,49].

Figure 4a shows the Nyquist plots for SPCE, GO/SPCE, rGO/SPCE, and IgG/rGO/SPCE conducted in a frequency range of 100 kHz to 0.1 Hz, a current range of 10 μA, and an amplitude of 20 mV. Based on the observed spectra, GO/SPCE shows the largest curve, followed by SPCE, while rGO/SPCE and IgG/rGO/SPCE have an almost similar linear curve from approximately 300 Ω onwards. The linear curves suggest that all electrode types are in a diffusion-limited process and are mainly influenced by the Warburg impedance owing to the low frequency. The Warburg impedance is typically characterized by a few assumptions; the electrode has a planar geometry, involves pure and semi-infinite diffusion, and is also based on Fick's law of diffusion [49]. In many cases where

 doi:10.20944/preprints201810.0631.v1

capacitance is the predominant term, the Nyquist plot (real vs. imaginary impedance) shows essentially a straight line, with emphasis on the low frequencies. Any graphical detail stemming from the high frequencies is therefore lost or negligible. One way to closely examine the contribution from high frequencies is to plot data in a manner similar to the Nyquist plot, but instead of real and imaginary impedance, to use the corresponding real and imaginary capacitance [50,51]. However, for the purpose of this study, we consider the low frequency plots. Figure 4b shows the slope and angle of the straight line observed in Figure 4a. The effect of impedance at the electrode surface can be observed by the slope and angle of the straight line, where a higher angle and slope indicate higher impedance. The bare SPCE, GO/SPCE, rGO/SPCE, and IgG/rGO/SPCE have slopes of 4.0165, 4.9833, 2.0315, and 2.3457, respectively; the angles of the linear curve of the SPCE, GO/SPCE, rGO/SPCE, and IgG/rGO/SPCE are 76.02°, 76.91°, 63.79°, and 64.98°, respectively. From the results, we can say that GO/SPCE has the highest impedance while rGO/SPCE and IgG/rGO/SPCE have the lowest and almost similar impedance. The results also suggest that the addition of IgG antibody serum does not have any significant effect on the transducer layer of rGO/SPCE. Fitting the EIS spectra with a Randles equivalent circuit, we determine that the charge-transfer resistance (R_{ct}) indicates the quantification of electron movement through experimental procedures for SPCE, GO/SPCE, rGO/SPCE, and IgG/rGO/SPCE is 36.29 kΩ, 60.51 kΩ, 5.23 kΩ and 3.55 kΩ, respectively. The results imply that the high impedance of GO/SPCE is due to the insulative properties of GO [52]. The addition of IgG to rGO/SPCE did not change the impedance by a significant amount.

There have been very limited studies on the use of EIS using SPCEs; current work with SPCEs focuses more on voltammetry techniques, making interpretation of our results challenging. Attachment of antibodies on microelectrode surfaces has shown to result in increased charge-transfer resistance on the electrode surface, and attachment of large *E. coli* cells greatly increased the charge-transfer resistance, as shown by the increase in the semicircle of a Nyquist plot [53]. However, those studies utilized microelectrodes, so the results obtained cannot be compared to those from our study. Significant differences can be seen from the shape of the Nyquist plots; our results show a significantly linear plot and an unnoticeable semi-circle. Studies have shown that immobilization of enzymes [54] or antibodies [55] increases R_{ct}; for studies with antibodies, increasing cell concentration did not yield a linear calibration plot [55]. However, these studies do not modify the surface of the SPCE with nanomaterials, whereas in our study, the SPCE surface was modified with rGO to increase surface area of the WE.

Preprints (www.preprints.org) | NOT PEER-REVIEWED | Posted: 26 October 2018 doi:10.20944/preprints201810.0631.v1

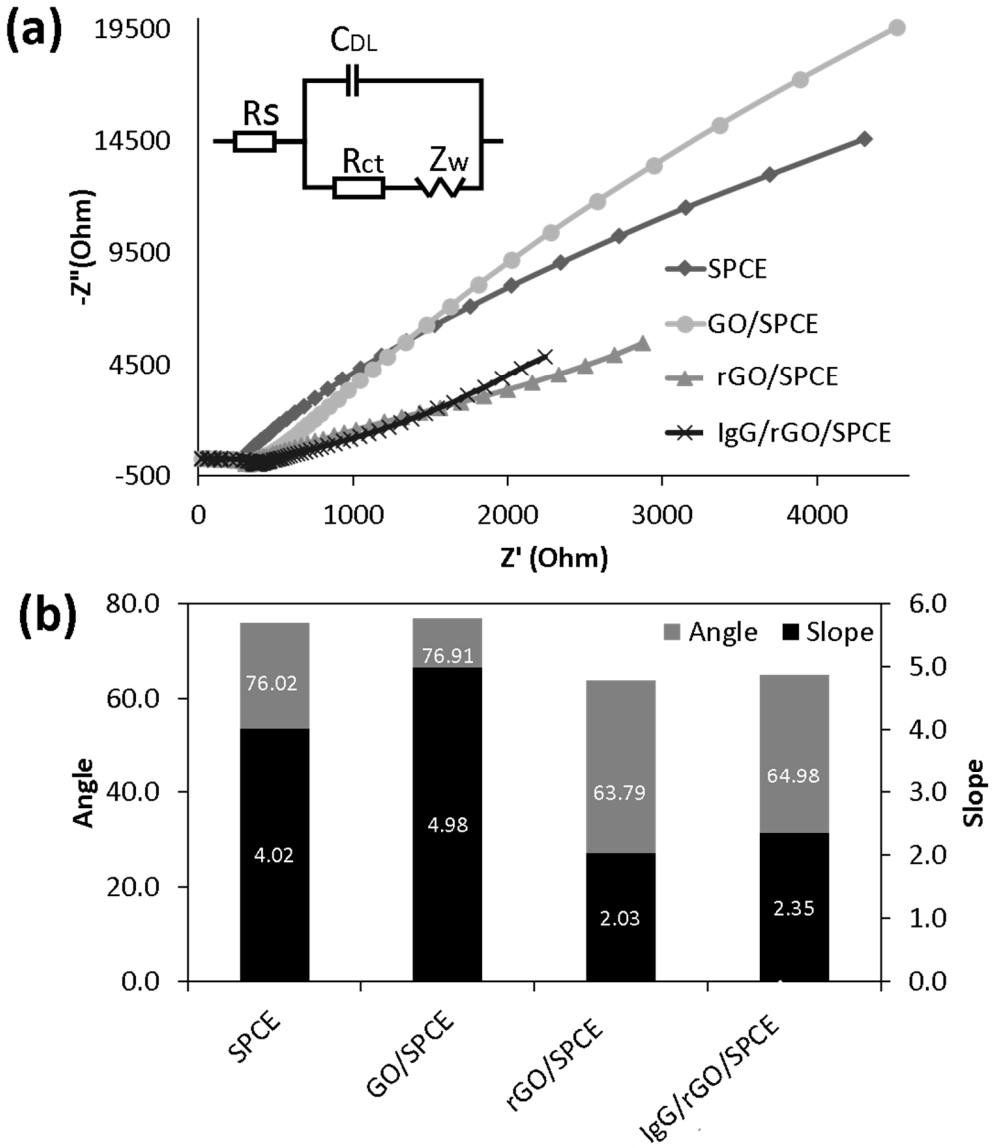

Figure 4 Nyquist plot for SPCEs with different materials deposited. (a) Impedance measurement for bare SPCE, GO/SPCE, rGO/SPCE, and with nonspecific antibody attachment, denoted as IgG/rGO/SPCE. Inset shows a typical Randles equivalent circuit. (b) Angle and slope of the linear curves extrapolated from the Nyquist plot for bare SPCE, GO/SPCE, rGO/SPCE, and with antibody attachment, denoted as IgG/rGO/SPCE. EIS measurements were performed in 0.01 M PBS, pH 7.1, containing 5 mM $K_3Fe(CN)_6$:$K_4Fe(CN)_6$ (1:1) with current range of 10 μA, amplitude of 20 mV, and frequency range of 100 kHz to 0.1 Hz.

3.3 LSV at different E. coli concentrations

LSV is used to quantify *E. coli* O157:H7 based on the electron transfer at the electrode surface where voltage is applied and the current measured is in response to attachment of *E. coli* cells on the electrodes.

Figure 5 shows LSVs of (a) IgG/rGO/SPCE and (b) rGO/SPCE with similar potential range for comparison. As can be seen from Figure 5a, graphs for *E. coli* concentration of 4×10^2 and 4×10^0 CFU/ml seems to overlap after the turning voltage of -0.14 V, and similarly for the higher concentrations. The lower current value of the hgiher concentration is attributed to higher cell

Preprints (www.preprints.org) | NOT PEER-REVIEWED | Posted: 26 October 2018 doi:10.20944/preprints201810.0631.v1

attachment to the rGO/SPCE, but the current value is not proportional to the *E. coli* concentration, probably as a result of weak affinity to the Fab region of IgG. From the results of both electrodes, we can say that higher cell attachment on the electrode surface resulted in lower current and that higher concentration of *E. coli* resulted in more nonspecific binding. Although the IgG used is not specific for *E. coli*, binding could occur even at low cell concentrations. Figure 5b shows the LSV graph for rGO/SPCE exposed to *E. coli* concentrations of 4×10^8, 4×10^5, 4×10^2, and 4×10^0 CFU/ml in tap water. As can be seen, LSV graphs seem to overlap for all *E. coli* concentrations. The results imply that without IgG, there is less binding of *E. coli* to the electrode surface, probably as a result of the rGO that can repel *E. coli* attachment [56,57]. Since a graphene-based surface is known to repel *E. coli* attachment, it can be said that IgG can attach to the *E. coli* surface through other mechanisms than the antibody-antigen complex.

Although we test the binding of *E. coli* for concentrations of 4×10^8 to 4×10^0 CFU/ml, we do not see a linear calibration curve. The random effect is believed to be a result of nonspecific binding, since the IgG used in this study is not specific to the strain of *E. coli* used. Several IgGs could also potentially bind to a single bacterium, which might lead to random orientation of the cells on the surface of the electrode. IgG could bind to several outer membrane constituents of the *E.coli*, including its lipopolysaccharides and porins. However, since the IgG used was not targeted at the specific strain, the binding affinity could be affected. Nonetheless, the LSV readings indicate that the bacterial cells are bound to the IgGs on the surface of the electrode, although the affinity and orientation of the bacteria may result in the absence of linearity in the LSV across different bacterial cell concentrations.

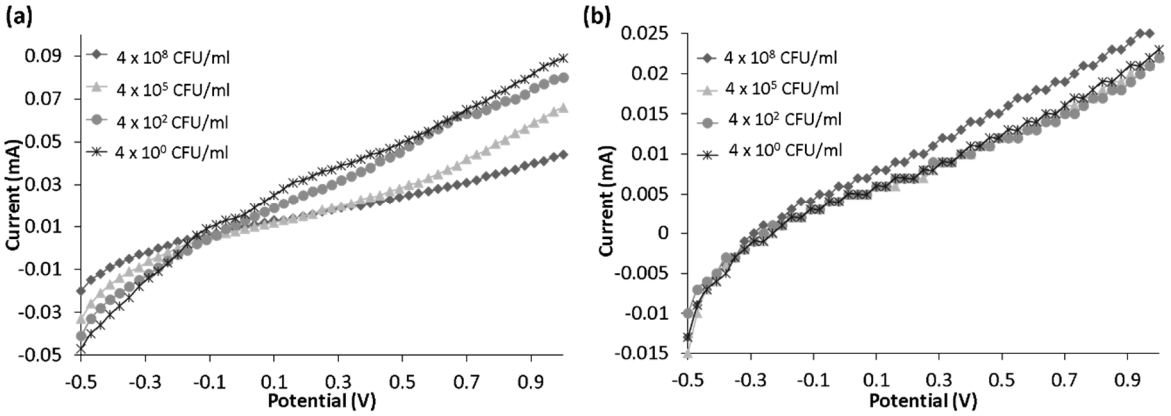

Figure 5 LSV graph of (a) /IgG/rGO/SPCE and (b) rGO/SPCE treated with different concentrations of *E. coli* (4×10^8, 4×10^5, 4×10^2, and 4×10^0 CFU/ml) in tap water at a scan rate of 100 mV/s.

3.4 EIS at different E. coli concentrations

EIS was used to study the impedance at the electrode-solution interface for *E. coli* concentrations of 4×10^8, 4×10^5, 4×10^2, and 4×10^0 CFU/ml for IgG/rGO/SPCE and rGO/SPCE. Various studies have shown employment of EIS to quantify bacteria concentration with high sensitivity and a wide linear range, when an antibody-antigen complex was used as the biorecognition layer [24]. In this study, IgG not specific for *E. coli* O157:H7 was used, and thus we expect nonspecific binding. However, it is interesting to see the effect of nonspecific binding on EIS measurements as LSV results showed that attachment on IgG-modified electrodes differed from that of electrodes not treated with IgG.

Figure 6 shows the Nyquist plot and corresponding slope and angle bar graphs for *E. coli* concentrations of 4×10^8, 4×10^5, 4×10^2, and 4×10^0 CFU/ml. Figures 6a and 6c show the Nyquist plot and the corresponding slope and angle bar graphs with IgG, where the highest slope and angle was for an *E.coli* concentration of 4×10^2 CFU/ml (slope = 1.715, angle = 61.28°), followed by 4×10^8 CFU/ml

Preprints (www.preprints.org) | NOT PEER-REVIEWED | Posted: 26 October 2018 doi:10.20944/preprints201810.0631.v1

(slope = 1.581, angle = 59.20°), 4 x 10^0 CFU/ml (slope = 1.535, angle = 56.92°), and 4 × 10^5 CFU/ml (slope = 1.361, angle = 53.70°); the random results imply nonspecific binding. Many studies have looked into the nonspecific binding of bacterial cells on biochips; the oxygenated silicon surface was found to adsorbed bacteria cells, so blocking agents are used [58]. However, even then limitations still exist in the form of nonspecific binding on biochip surfaces, as antibodies can undergo structural changes and affect sensor sensitivity. It is important to note that this is not solely a limitation of electrochemical biosensors, but is shared by optical sensors [59]

The results of our study strongly suggest that control experiments are important when utilizing electrochemical sensors for bacteria detection, to avoid nonspecific bacteria adsorption that results in false measured signals. As a control, we performed EIS on the rGO/SPCE surface, without the presence of IgG. Figures 6b and 6d show the Nyquist plot and the corresponding slope and angle bar graphs for *E. coli* concentrations of 4 × 10^8, 4 × 10^5, 4 × 10^2, and 4 × 10^0 CFU/ml. As can be seen, the slope and angle follow a linear calibration profile, where higher concentration of *E. coli* resulted in higher slope and angle, with the highest slope and angle for 4 × 10^8 CFU/ml (slope = 2.23, angle = 65.80°), followed by 4 × 10^5 CFU/ml (slope = 2.12, angle = 64.77°), 4 × 10^2 CFU/ml (slope = 2.06, angle = 64.05°), and *E.coli* concentration 4 × 10^0 CFU/ml (slope = 2.05, angle = 64.02°) with the lowest slope and angle. This result is interesting because it shows that IgG seems to contribute to the random attachment of *E. coli* on the electrodes. Random attachment of cells on IgG/rGO/SPCE could be the result of IgG's having residual binding sites that could contribute to the random attachment. In our experiments, the IgG amine groups of the heavy chain Fc region are believed to bind to the carboxyl groups available on the rGO surface, so the Fab regions are exposed to bind to targeted analyte.

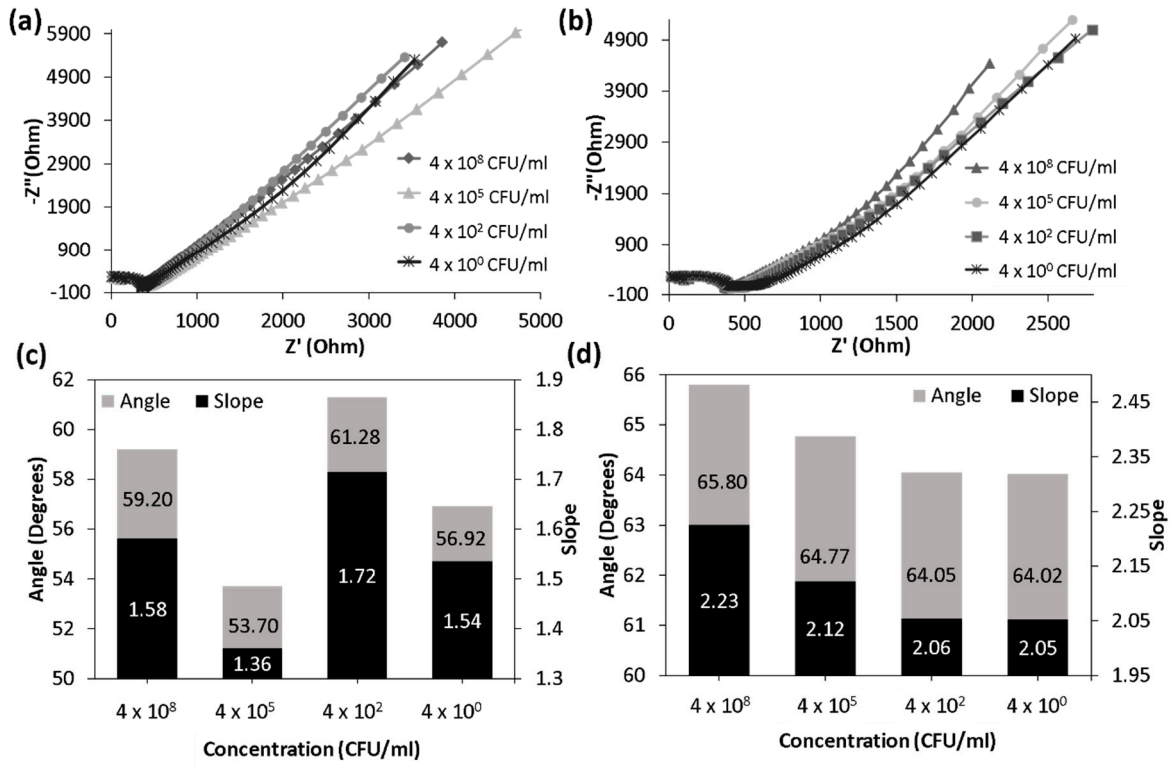

Figure 6 shows Nyquist plot at *E.coli* concentration of 4 × 10^8, 4 × 10^5, 4 × 10^2, and 4 × 10^0 CFU/ml for (a) IgG/rGO/SPCE with corresponding angle and slope (b), and (c) rGO/SPCE with corresponding angle and slope (d). All EIS were measured in 0.01 M PBS, pH 7.1, containing 5 mM $K_3Fe(CN)_6$:$K_4Fe(CN)_6$ (1:1) as redox probe with current range of 10 µA, amplitude of 20 mV, and frequency range of 100 kHz to 0.1 Hz.

 doi:10.20944/preprints201810.0631.v1

3.5 FESEM to verify attachment of E. coli on electrode surfaces

FESEM analysis was performed to confirm the attachment of *E. coli* (4×10^7 and 4×10^5 CFU/ml) on electrode surfaces for IgG/rGO/SPCE and rGO/SPCE for four quadrants of a Ø=2 mm WE. As can be seen in Figure 7, for both electrode types, higher concentration of *E. coli* resulted in higher binding, although more cells can be seen attach to the IgG-modified surface for the 4×10^7 CFU/ml concentration (Figure 7a, ABCD). For the lower concentration, the FESEM image is almost similar for both electrodes. The results of the FESEM imply that nonspecific binding occurs more with higher *E. coli* concentration. Owing to the enhanced effect of nonspecific binding at higher concentration, a prefiltration step is deemed necessary. Furthermore, a differential approach of subtracting the sensor response between a reference sensor (without antibody) and with antibody can be used to remove false signals. The sensors should also be rinsed with buffer solution prior to measurement to remove loosely attached antibodies. Alternatively, introducing a common protein blocking agents such as bovine serum albumin, skimmed milk, or non-ionic detergent such as Tween-20 or Triton X-100 may also remove nonspecific binding [60].

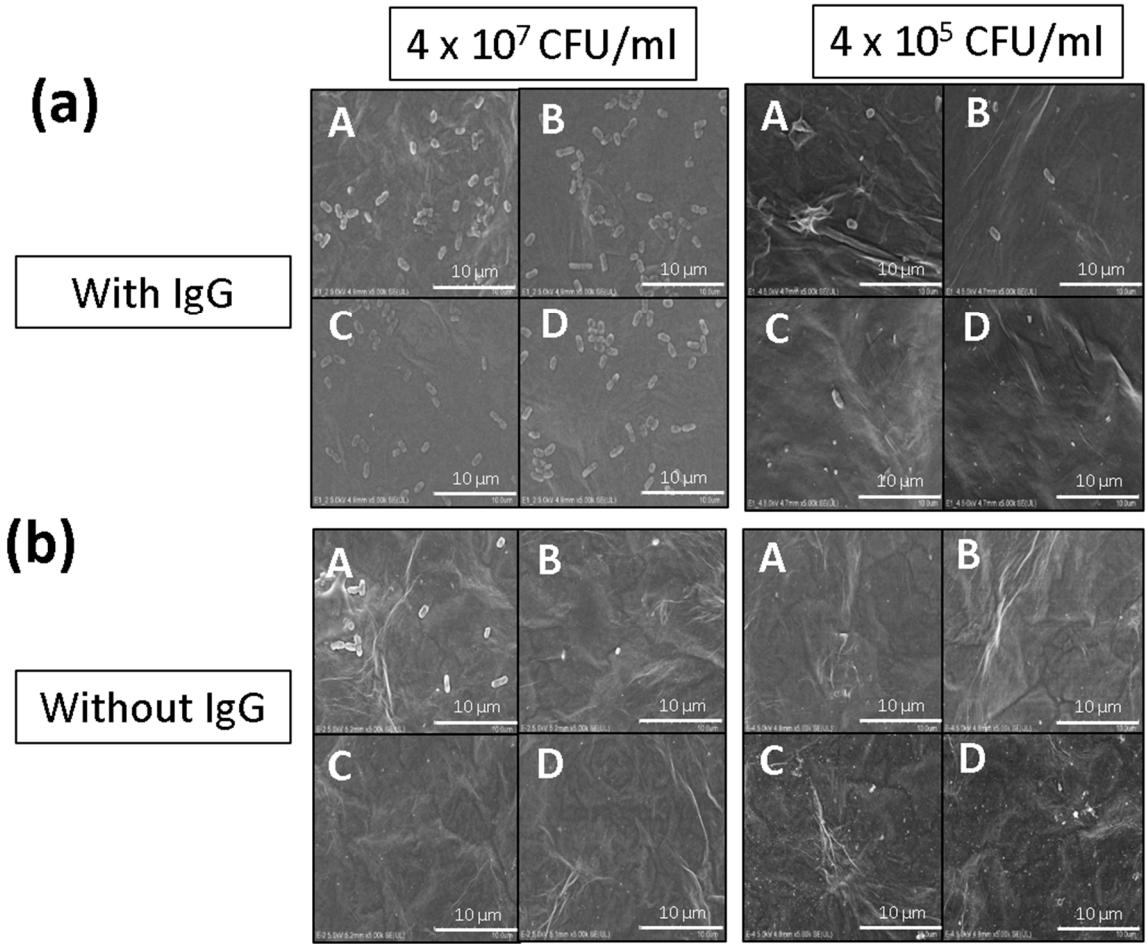

Figure 7 FESEM images showing cell attachment on electrode surface for measurements made in tap water samples of antibody for *E. coli* concentrations of 4×10^7 and 4×10^5 CFU/ml. (a) IgG/rGO/SPCE. (b) rGO/SPCE. FESEM images were taken for quadrants of a Ø=2 mm SPCE.

5. Conclusions

The results of the study show the effect of nonspecific binding reflected in LSV and EIS when IgG was used as a model antibody. IgG antibody was chosen to be nonspecific with respect to the *E. coli* O157:H7 strain to introduce no specificity in the binding. LSV and EIS results for IgG/rGO/SPCE

was compared to that of rGO/SPCE, the latter with absence of IgG. For LSV, there is a change in current from the bare SPCEs at all cell concentrations for IgG/rGO/SPCE while no change in current could be seen for all concentrations for rGO/SPCE. FESEM results reveal more binding of *E. coli* on rGO/SPCE with IgG in comparison with rGO/SPCE without IgG. The binding of *E. coli* on the electrode surface still occurs at the lowest concentration of *E. coli*, 4 CFU/ml. However, there is no linear relationship between current and *E. coli* concentration for IgG/rGO/SPCE samples owing to the random effect introduced by the nonspecific binding. The results of the study suggest that nonspecific binding of cells on electrode surfaces can introduce false electrochemical signals. Electrochemical methods are not able to differentiate between living and dead cells, but they are sensitive to any changes in the electrode surface. Since quantification is the key in biosensing, it is important to reduce nonspecific binding, and efforts are likewise needed to understand the mechanism of bacterial attachment to electrode surfaces. Microfluidics with prefiltration steps and proper controls can enable the use of modified SPCE for bacteria detection. Furthermore, more studies are needed to understand the effect of nanomaterials on impedance at the electrode-solution interface.

Author Contributions: Conceptualization, Wan Wardatul Amani Wan Salim; Data curation, Nur Alya Batrisya Ismail, Nasteho Ali Ahmed, Nurul Izzati Ramli and Wan Wardatul Amani Wan Salim; Formal analysis, Nur Alya Batrisya Ismail, Nasteho Ali Ahmed, Firdaus Abd-Wahab, Nurul Izzati Ramli and Wan Wardatul Amani Wan Salim; Funding acquisition, Wan Wardatul Amani Wan Salim; Investigation, Nur Alya Batrisya Ismail, Nasteho Ali Ahmed and Wan Wardatul Amani Wan Salim; Methodology, Nur Alya Batrisya Ismail, Nasteho Ali Ahmed, Firdaus Abd-Wahab and Wan Wardatul Amani Wan Salim; Project administration, Wan Wardatul Amani Wan Salim; Resources, Wan Wardatul Amani Wan Salim; Supervision, Wan Wardatul Amani Wan Salim; Validation, Nur Alya Batrisya Ismail, Firdaus Abd-Wahab and Wan Wardatul Amani Wan Salim; Visualization, Nur Alya Batrisya Ismail, Firdaus Abd-Wahab and Nurul Izzati Ramli; Writing – original draft, Nur Alya Batrisya Ismail, Firdaus Abd-Wahab, Nurul Izzati Ramli and Wan Wardatul Amani Wan Salim; Writing – review & editing, Wan Wardatul Amani Wan Salim.

Funding: This research was funded by The Royal Society Travel Grant, and IIUM Postdoctoral Research Initiative Grant Scheme.

Conflicts of Interest: The authors declare no conflict of interest. The funders had no role in the design of the study; in the collection, analysis, or interpretation of data; in the writing of the manuscript; or in the decision to publish the results.

References

1. Kosack, C. S.; Page, A.-L.; Klatser, P. R. A guide to aid the selection of diagnostic tests. *Bull. World Health Organ.* **2017**, *95*, 639–645, doi:10.2471/BLT.16.187468.

2. Tam, P. D.; Van Hieu, N.; Chien, N. D.; Le, A. T.; Anh Tuan, M. DNA sensor development based on multi-wall carbon nanotubes for label-free influenza virus (type A) detection. *J. Immunol. Methods* **2009**, *350*, 118–124, doi:10.1016/j.jim.2009.08.002.

3. Li, X.; Scida, K.; Crooks, R. M. Detection of Hepatitis B virus DNA with a paper electrochemical sensor. *Anal. Chem.* **2015**, *87*, 9009–9015, doi:10.1021/acs.analchem.5b02210.

4. Xu, S.; Zhang, Y.; Dong, K.; Wen, J.; Zheng, C.; Zhao, S. Electrochemical DNA biosensor based on graphene oxide-chitosan hybrid nanocomposites for detection of Escherichia coli O157:H7. *Int. J. Electrochem. Sci.* **2017**, *12*, 3443–3458, doi:10.20964/2017.04.16.

5. Byrne, B.; Stack, E.; Gilmartin, N.; O'Kennedy, R. Antibody-based sensors: Principles, problems and potential for detection of pathogens and associated toxins. *Sensors (Switzerland)*

2009, *9*, 4407–4445, doi:10.3390/s90604407.

6. Malvano, F.; Pilloton, R.; Albanese, D. Sensitive detection of Escherichia coli O157:H7 in food products by impedimetric immunosensors. *Sensors* **2018**, *18*, 2168, doi:10.3390/s18072168.

7. Wen, T.; Wang, R.; Sotero, A.; Li, Y. A portable impedance immunosensing system for rapid detection of Salmonella Typhimurium. *Sensors (Switzerland)* **2017**, *17*, 1–15, doi:10.3390/s17091973.

8. Kaneko, N.; Horii, K.; Akitomi, J.; Kato, S.; Shiratori, I.; Waga, I.; Kaneko, N.; Horii, K.; Akitomi, J.; Kato, S.; Shiratori, I.; Waga, I. An aptamer-based biosensor for direct, label-free detection of melamine in raw milk. *Sensors* **2018**, *18*, 3227, doi:10.3390/S18103227.

9. Ortiz-aguayo, D.; Valle, M. del Label-free aptasensor for lysozyme detection using electrochemical impedance spectroscopy. *Sensors* **2018**, *18*, 354, doi:10.3390/s18020354.

10. Mao, Y.; Chen, Y.; Li, S.; Lin, S.; Jiang, Y. A graphene-based biosensing platform based on regulated release of an aptameric DNA biosensor. *Sensors (Switzerland)* **2015**, *15*, 28244–28256, doi:10.3390/s151128244.

11. Mannoor, M. S.; Zhang, S.; Link, A. J.; McAlpine, M. C. Electrical detection of pathogenic bacteria via immobilized antimicrobial peptides. *Proc. Natl. Acad. Sci.* **2010**, *107*, 19207–19212, doi:10.1073/pnas.1008768107.

12. Li, Y.; Afrasiabi, R.; Fathi, F.; Wang, N.; Xiang, C.; Love, R.; She, Z.; Kraatz, H. B. Impedance based detection of pathogenic E. coli O157: H7 using a ferrocene-antimicrobial peptide modified biosensor. *Biosens. Bioelectron.* **2014**, *58*, 193–199, doi:10.1016/j.bios.2014.02.045.

13. Lillehoj, P. B.; Kaplan, C. W.; He, J.; Shi, W.; Ho, C. M. Rapid, electrical impedance detection of bacterial pathogens using immobilized antimicrobial peptides. *J. Lab. Autom.* **2014**, *19*, 42–49, doi:10.1177/2211068213495207.

14. Ma, F.; Rehman, A.; Liu, H.; Zhang, J.; Zhu, S.; Zeng, X. Glycosylation of quinone-fused polythiophene for reagentless and label-free detection of E. coli. *Anal. Chem.* **2015**, *87*, 1560–1568, doi:10.1021/ac502712q.

15. Guo, X.; Kulkarni, A.; Doepke, A.; Halsall, H. B.; Iyer, S.; Heineman, W. R. Carbohydrate-based label-free detection of *Escherichia coli* ORN 178 using electrochemical impedance spectroscopy. *Anal. Chem.* **2012**, *84*, 241–246, doi:10.1021/ac202419u.

16. Neufeld, T.; Schwartz-Mittelmann, A.; Biran, D.; Ron, E. Z.; Rishpon, J. Combined phage typing and amperometric detection of released enzymatic activity for the specific identification and quantification of bacteria. *Anal. Chem.* **2003**, *75*, 580–585, doi:10.1021/ac026083e.

17. Neufeld, T.; Mittelman, A. S.; Buchner, V.; Rishpon, J. Electrochemical phagemid assay for the specific detection of bacteria using *Escherichia coli* TG-1 and the M13KO7 phagemid in a

model system. *Anal. Chem.* **2005**, *77*, 652–657, doi:10.1021/ac0488053.

18. Shabani, A.; Zourob, M.; Allain, B.; Marquette, C. A.; Lawrence, M. F.; Mandeville, R. Bacteriophage-modified microarrays for the direct impedimetric detection of bacteria. *Anal. Chem.* **2008**, *80*, 9475–9482, doi:10.1021/ac801607w.

19. Griffin, P. M.; Tauxe, R. V. The Epidemiology of infections caused by *Escherichia coli* O157: H7, other enterohemorrhagic *E. coli*, and the associated hemolytic uremic syndrome. *Epidemiol. Rev.* **1991**, *13*, 60–98, doi:10.1093/oxfordjournals.epirev.a036079.

20. Sandvig, K.; Grimmer, S.; Lauvrak, S.; Torgersen, M.; Skretting, G.; Van Deurs, B.; Iversen, T. Pathways followed by ricin and Shiga toxin into cells. *Histochem. Cell Biol.* **2002**, *117*, 131–141, doi:10.1007/s00418-001-0346-2.

21. Callaway, T. R.; Carr, M. A.; Edrington, T. S.; Anderson, R. C.; Nisbet, D. J. Diet, *Escherichia coli* O157: H7, and cattle: a review after 10 years. *Curr Issues Mol Biol* **2009**, *11*, 67–80.

22. Janisiewicz, W. J.; Conway, W. S.; Brown, M. W.; Sapers, G. M.; Fratamico, P.; Buchanan, R. L. Fate of *Escherichia coli* O157:H7 on fresh-cut apple tissue and its potential for transmission by fruit flies. *Appl. Environ. Microbiol.* **1999**, *65*, 1–5.

23. Basri, Z. D. M.; Othman, Z.; Wahid, M. A. Quantification of pathogenic bacteria in flood water in Malaysia. In *5th International Conference on Geotechnique, Construction Materials and Environment*; Osaka, Japan, 2016; pp. 14–18.

24. Amiri, M.; Bezaatpour, A.; Jafari, H.; Boukherroub, R.; Szunerits, S. Electrochemical methodologies for the detection of pathogens. *ACS Sensors* **2018**, doi:10.1021/acssensors.8b00239.

25. Rispens, T.; Vidarsson, G. Human IgG Subclasses. In *Antibody Fc*; Elsevier Inc., **2014**; pp. 159–177 ISBN 9780123948021.

26. Alberts, B.; Johnson, A.; Lewis, J.; Raff, M.; Roberts, K.; Walter, P. B cells and antibodies.In *Molecular biology of the cell*; 4th Edition. New York: Garland Science, **2002** ISBN 978-0-8153-4105-5.

27. Mak, T. W.; Saunders, M. E. *The immune response: basic and clinical principles*; 1st Edition; Elsevier Academic Press: London, UK, **2006**; ISBN 9780120884513.

28. Schager, A. E.; Dominguez-Medina, C. C.; Necchi, F.; Micoli, F.; Goh, Y. S.; Goodall, M.; Flores-Langarica, A.; Bobat, S.; Cook, C. N. L.; Arcuri, M.; Marini, A.; King, L. D. W.; Morris, F. C.; Anderson, G.; Toellner, K. M.; Henderson, I. R.; López-Macías, C.; MacLennan, C. A.; Cunningham, A. F. IgG responses to porins and lipopolysaccharide within an outer membrane-based vaccine against nontyphoidal Salmonella develop at discordant rates. *Am. Soc. Microbiol.* **2018**, *9*, 1–15, doi:10.1128/mBio.02379-17.

29. Arris, F. A.; Ithnin, M. H.; Wan Salim, W. W. A. Characterizing graphene-modified electrodes

for interfacing with Arduino -based devices. In *2016 38th Annual International Conference of the IEEE Engineering in Medicine and Biology Society (EMBC)*; IEEE: Orlando, FL, USA, **2016**; pp. 4937–4940.

30. Fei, J.; Dou, W.; Zhao, G. Amperometric immunoassay for the detection of Salmonella pullorum using a screen-printed carbon electrode modified with gold nanoparticle-coated reduced graphene oxide and immunomagnetic beads. *Microchim. Acta* **2016**, *183*, 757–764, doi:10.1007/s00604-015-1721-3.

31. Guthoos, H. F. A.; Noorin, N. N.; Ismail, N. A. B.; Tumian, A.; Wan Salim, W. W. A. Effect of gold nanoparticles and electrode drying time on reduced graphene oxide-based composite with respect to peak current of cyclic voltammetry. *ARPN J. Eng. Appl. Sci.* **2018**, *13*, 1420–1426.

32. Ong, C.; Ibrahim, S.; Sen Gupta, B. A survey of tap water quality in Kuala Lumpur. *Urban Water J.* **2007**, *4*, 29–41, doi:10.1080/15730620601145923.

33. Parker, V. D. Linear sweep and cyclic voltammetry. In *Comprehensive Chemical Kinetics*; **1986**; Vol. 26, pp. 145–202 ISBN 9780444425508.

34. Gu, W.; Wang, Y.; Wu, T.; Li, W.; Wang, H.; Xia, W. Linear sweep voltammetric studies on the complex of alizarin red s with aloe polysaccharide and determination of aloe polysaccharide. *Carbohydr. Res.* **2012**, *349*, 82–85, doi:10.1016/j.carres.2011.11.026.

35. Jung, J. H.; Cheon, D. S.; Liu, F.; Lee, K. B.; Seo, T. S. A Graphene oxide based immuno-biosensor for pathogen detection. *Angew. Chemie Int. Ed.* **2010**, *49*, 5708–5711, doi:10.1002/anie.201001428.

36. Lisdat, F.; Schäfer, D. The use of electrochemical impedance spectroscopy for biosensing. *Anal. Bioanal. Chem.* **2008**, *391*, 1555–1567, doi:10.1007/s00216-008-1970-7.

37. Barreiros dos Santos, M.; Agusil, J. P.; Prieto-Simón, B.; Sporer, C.; Teixeira, V.; Samitier, J. Highly sensitive detection of pathogen Escherichia coli O157: H7 by electrochemical impedance spectroscopy. *Biosens. Bioelectron.* **2013**, *45*, 174–180, doi:10.1016/j.bios.2013.01.009.

38. Wang, J.; Pedrero, M.; Sakslund, H.; Hammerich, O. Electrochemical activation of screen-printed carbon strips. *Analyst* **1996**, *121*, 345–350.

39. Screen printed electrode information: Carbon and ceramic electrode information. *Pine Research Instruments*. **2016**, pp. 1–10. Retrieval date: 26 October 2018. www.pineresearch.com

40. Pei, S.; Cheng, H. M. The reduction of graphene oxide. *Carbon N. Y.* **2012**, *50*, 3210–3228, doi:10.1016/j.carbon.2011.11.010.

41. Randviir, E. P.; Banks, C. E. The oxygen reduction reaction at graphene modified electrodes. *Electroanalysis* **2014**, *26*, 76–83, doi:10.1002/elan.201300477.

42. Pumera, M. *Materials Today*. Elsevier Ltd **2011**, pp. 308–315.

43. Childres, I.; Jauregui, L.; Park, W.; Cao, H.; Chen, Y. Raman spectroscopy of graphene and related materials. *New Dev. Phot. Mater. Res.* **2013**, 1–20, doi:10.1016/B978-0-444-53175-9.00016-7.

44. Lawal, A. T. Synthesis and utilisation of graphene for fabrication of electrochemical sensors. *Talanta* **2015**, *131*, 424–443, doi:10.1016/j.talanta.2014.07.019.

45. Rosenberg, B. Electrical conductivity of protein. *Nature* **1962**, *193*, 364–365.

46. Zhang, X. Y.; Shao, J.; Jiang, S. X.; Wang, B.; Zheng, Y. Structure-dependent electrical conductivity of protein: Its differences between alpha-domain and beta-domain structures. *Nanotechnology* **2015**, *26*, 125702, doi:10.1088/0957-4484/26/12/125702.

47. Abd Azes, N. I.; Yusoff, N. H.; Najmi, N.; Sulaiman, K. S.; Sulaiman, M. A. Conductivity and electrochemical study of non-aqueous NaPF6 electrolyte in organic solvent mixture for sodium-ion batteries. *J. Ind. Technol.* **2017**, *25*, 19–28, doi:10.21908/jit.2017.4.

48. Ngamchuea, K.; Eloul, S.; Tschulik, K.; Compton, R. G. Planar diffusion to macro disc electrodes—what electrode size is required for the Cottrell and Randles-Sevcik equations to apply quantitatively? *J. Solid State Electrochem.* **2014**, *18*, 3251–3257, doi:10.1007/s10008-014-2664-z.

49. Huang, J. Diffusion impedance of electroactive materials, electrolytic solutions and porous electrodes: Warburg impedance and beyond. *Electrochim. Acta* **2018**, *281*, 170–188, doi:10.1016/j.electacta.2018.05.136.

50. Fernandes, F. C. B.; Santos, A.; Martins, D. C.; Góes, M. S.; Bueno, P. R. Comparing label free electrochemical impedimetric and capacitive biosensing architectures. *Biosens. Bioelectron.* **2014**, *57*, 96–102, doi:10.1016/j.bios.2014.01.044.

51. Fernandes, F. C. B.; Góes, M. S.; Davis, J. J.; Bueno, P. R. Label free redox capacitive biosensing. *Biosens. Bioelectron.* **2013**, *50*, 437–440, doi:10.1016/j.bios.2013.06.043.

52. Pei, S.; Cheng, H. M. The reduction of graphene oxide. *Carbon N. Y.* **2012**, *50*, 3210–3228, doi:10.1016/j.carbon.2011.11.010.

53. Siddiqui, S.; Dai, Z.; Stavis, C. J.; Zeng, H.; Moldovan, N.; Hamers, R. J.; Carlisle, J. A.; Arumugam, P. U. A quantitative study of detection mechanism of a label-free impedance biosensor using ultrananocrystalline diamond microelectrode array. *Biosens. Bioelectron.* **2012**, *35*, 284–290, doi:10.1016/j.bios.2012.03.001.

54. Lu, B. W.; Chen, W. C. A disposable glucose biosensor based on drop-coating of screen-printed carbon electrodes with magnetic nanoparticles. *J. Magn. Magn. Mater.* **2006**, *304*, 400–402, doi:10.1016/j.jmmm.2006.01.222.

55. Balkenhohl, T.; Lisdat, F. Screen-printed electrodes as impedimetric immunosensors for the detection of anti-transglutaminase antibodies in human sera. *Anal. Chim. Acta* **2007**, *597*, 50–57, doi:10.1016/j.aca.2007.06.041.

56. Kurantowicz, N.; Sawosz, E.; Jaworski, S.; Kutwin, M.; Strojny, B.; Wierzbicki, M.; Szeliga, J.; Hotowy, A.; Lipińska, L.; Koziński, R.; Jagiełło, J.; Chwalibog, A. Interaction of graphene family materials with Listeria monocytogenes and Salmonella enterica. *Nanoscale Res. Lett.* **2015**, *10*, 1–12, doi:10.1186/s11671-015-0749-y.

57. Nanda, S. S.; Yi, D. K.; Kim, K. Study of antibacterial mechanism of graphene oxide using Raman spectroscopy. *Sci. Rep.* **2016**, *6*, 1–12, doi:10.1038/srep28443.

58. Huang, T. T.; Sturgis, J.; Gomez, R.; Geng, T.; Bashir, R.; Bhunia, A. K.; Robinson, J. P.; Ladisch, M. R. Composite surface for blocking bacterial adsorption on protein biochips. *Biotechnol. Bioeng.* **2003**, *81*, 618–624, doi:10.1002/bit.10507.

59. Banada, P. P.; Bhunia, A. K. Antibodies and immunoassays for detection of bacterial pathogens. In *Principles of Bacterial Detection*; Zourob, M., Elwary, S., Turner, A., Eds.; Springer Science: New York, NY, USA, **2014**; pp. 567–595 ISBN 9780387751122.

60. Banica, F.-G. *Chemical Sensors and Biosensors*; Fogg, A. G., Ed.; 1st Edition; John Wiley & Sons Ltd.: Chichester, West Sussex, United Kingdom, **2012**; ISBN 978-0-470-71066-1.